Separation Science and Technology
Publication details, including instructions for authors and subscription information:
http://www.informaworld.com/smpp/title~content=t713708471

Separation of Cells and Cell-Sized Particles by Continuous SPLITT Fractionation Using Hydrodynamic Lift Forces

Jue Zhang[a]; P. Stephen Williams[a]; Marcus N. Myers[a]; J. Calvin Giddings[a]
[a] FIELD-FLOW FRACTIONATION RESEARCH CENTER, DEPARTMENT OF CHEMISTRY, UNIVERSITY OF UTAH, SALT LAKE CITY, UTAH

To cite this Article Zhang, Jue , Williams, P. Stephen , Myers, Marcus N. and Giddings, J. Calvin(1994) 'Separation of Cells and Cell-Sized Particles by Continuous SPLITT Fractionation Using Hydrodynamic Lift Forces', Separation Science and Technology, 29: 18, 2493 — 2522
To link to this Article: DOI: 10.1080/01496399408002205
URL: http://dx.doi.org/10.1080/01496399408002205

SEPARATION SCIENCE AND TECHNOLOGY, 29(18), pp. 2493–2522, 1994

Separation of Cells and Cell-Sized Particles by Continuous SPLITT Fractionation Using Hydrodynamic Lift Forces

JUE ZHANG, P. STEPHEN WILLIAMS, MARCUS N. MYERS, and J. CALVIN GIDDINGS*
FIELD-FLOW FRACTIONATION RESEARCH CENTER
DEPARTMENT OF CHEMISTRY
UNIVERSITY OF UTAH
SALT LAKE CITY, UTAH 84112

ABSTRACT

The use of hydrodynamic lift forces for the separation of particles according to size by continuous SPLITT fractionation is explored. The mechanism for particle separation in the transport mode of SPLITT fractionation is first explained. This is followed by a discussion of the hydrodynamic lift forces that act upon particles entrained in fluid flow between the parallel bounding walls of the SPLITT cell. The effect of the bounding walls on particle motion both parallel and perpendicular to the direction of flow is explained. Computer simulations of particle trajectories are presented that predict extremely high size selectivity for the method. A parallel experimental study was carried out using both polystyrene latex particles and red blood cells. The experimental selectivity was found to be smaller than that predicted theoretically. This discrepancy is attributable to nonidealities in the construction of the SPLITT cell. Nonetheless, the results are promising. Suspensions of polystyrene particle standards (from 2 to 50 μm in diameter) demonstrate that fast and relatively clean size separations are possible provided particles differ sufficiently in size and flow conditions are properly optimized. It is also shown that the system has the potential to quickly and gently separate blood cells from plasma.

* Corresponding author.

INTRODUCTION

A split-flow thin (SPLITT) separation cell is a thin (generally submillimeter) rectangular channel in which various physical forces are utilized to drive components differentially across the thin dimension of the channel, generally from one major wall toward the opposite wall (1, 2). At the same time, a film of fluid flowing lengthwise through the channel causes the rapid longitudinal displacement of entrained components. By introducing a flow splitter at the downstream end of the channel, precisely positioned to split the flowing film into two constituent lamina, the suspended material can be separated into two substreams (or fractions) whose compositions depend upon the fine tuning of substream flow rates and driving forces (1). The separation process is called SPLITT fractionation (SF). This separative operation is characterized by an intrinsically high resolving power, an extraordinarily high speed (because of the short transport path—the order of 100 μm—needed for separation), a relatively simple theoretical description, and a great deal of versatility resulting from the large variety of driving forces and flow configurations that can be used. Importantly, the SPLITT cell can be used for continuous fractionation, a process referred to as continuous SPLITT fractionation (CSF). The capability for the continuous operation of SF systems distinguishes this methodology from its relative, field-flow fractionation (FFF), which is limited to batch (discrete) operation. The techniques of CSF and FFF have been compared in recent publications (2, 3).

A number of different driving forces have been utilized to implement CSF. The first implementation was based on gravitational sedimentation (4). Subsequent experimental studies have been based on diffusive transport (5, 6) and electrically driven transport (7). We have also realized CSF in a centrifugal SPLITT cell (8). Other forces have been discussed as a basis of CSF. Most importantly for present purposes is a recent analysis of the potential of using hydrodynamic lift forces in association with SPLITT cells (9). These forces can be used in unique ways because of their nonuniformity; the magnitude of the applied force varies rapidly over the channel thickness.

The object of this study is to examine by experimental means the fractionation of micron-sized particles using a SPLITT channel in which hydrodynamic lift forces are the dominant forces affecting particle transport. (In principle, hydrodynamic lift forces can be combined with other forces to generate separation as well.) More specifically, our goal is to achieve a transport-based separation in which particles of different sizes are transported at different rates away from a designated channel wall as a consequence of lift forces. An equilibrium-based (as opposed to transport-

based) separation is expected to work poorly without the intervention of other forces, because particles of different sizes tend to accumulate at nearly identical distances from the wall once equilibrium is reached (10–12). The rate of transport toward the equilibrium position, however, is highly sensitive to particle diameter, having between a first and third power dependence (9). Thus lift-based transport should be highly size selective.

The concept of utilizing hydrodynamic lift forces in the transport mode is illustrated in Fig. 1. This figure represents the relevant features of separation as viewed from one edge of the channel; however, the thickness (w) of the channel is greatly exaggerated relative to its length (L) in order to illustrate transport along this thin dimension. (The aspect ratio, L/w, is typically 100 to 500.) The system is characterized by an inlet splitter

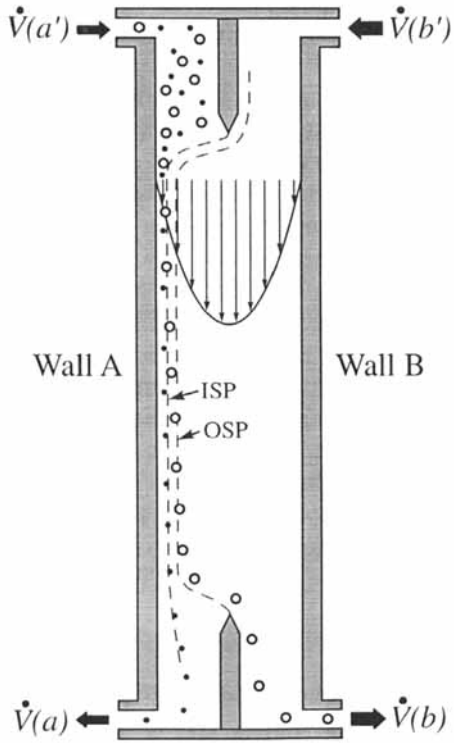

FIG. 1 Edge view of SPLITT cell using hydrodynamic lift forces to separate particles. Carrier flow is in the downward direction. A representation of the parabolic velocity profile across the cell thickness, and the positions of the inlet and outlet splitting planes (ISP and OSP, respectively) are shown.

that serves to compress the incoming (feed) particle stream into a thin band near wall A. The degree of compression is determined by the ratio of the flow rates of inlet streams b' and a'; increasing values of this ratio lead to increasingly thin initial particle bands (5, 9). The thickness of this particle-containing lamina is fixed by wall A (at position $x = 0$) bounding the lamina on one side and by the position of the inlet splitting plane (at $x = w_{a'}$) forming the opposite boundary plane.

The thin particle-containing lamina formed just beyond the inlet splitter is subject to a loss of material by various transport processes which, depending upon circumstances, may include sedimentation, diffusion, and lift forces. Sedimentation effects can be virtually eliminated by turning the channel on one end so that the flow and gravity axes are parallel. Diffusion is generally negligible when using large particles. In these circumstances, lift forces alone govern the transport of particles across the boundary of the initially confined lamina. Large particles are expected to be driven more rapidly away from the proximal wall by lift forces than are the small particles.

To utilize this differential transport, an outlet splitter must be installed. In this case the position of the outlet splitting plane (the plane dividing fluid elements destined to emerge at outlets a and b) is governed by the ratio of the flow rates from outlet substreams a and b. This splitting plane, because of its positional dependence upon a controllable flow ratio, can be "tuned" up and down to most effectively skim off the larger particles and force their removal from a different outlet (b) than that exited by the smaller particles. Thus, in principle, a particle stream can be divided into two component streams, one containing particles above a critical diameter d_c (whose magnitude depends upon the channel dimensions and flow conditions) and the other containing smaller particles. (Other cutoff diameters can be used in subsequent passes or in downstream SPLITT cells to generate increasingly narrow size distributions.)

In this paper the above concept will be experimentally implemented and its efficiency tested. Its theoretical description will be further refined relative to that provided in the original publication (9).

THEORETICAL BACKGROUND

SPLITT Cell Conventions

The plane walls are specified as A and B. For implementation of the transport mode of operation the sample substream is introduced at inlet a' adjacent to wall A at a flow rate of $\dot{V}(a')$. Pure carrier is introduced at inlet b' adjacent to wall B at a flow rate of $\dot{V}(b')$. During passage through the system, sample components migrate at different rates toward wall B.

Substreams having flow rates of $\dot{V}(a)$ and $\dot{V}(b)$ are withdrawn at outlets a and b, adjacent to walls A and B, respectively. Mass conservation requires that the total flow rate $\dot{V}$ through the system is the sum

$$\dot{V} = \dot{V}(a') + \dot{V}(b') = \dot{V}(a) + \dot{V}(b) \tag{1}$$

Distance x across the cell thickness w is measured from wall A. Transverse forces and particle velocities are positive in the direction of the x-axis. The z-axis runs along the length of the cell in the direction of flow. The origin is placed at the edge of the inlet splitter where the inlet substreams merge, and the edge of the outlet splitter where the outlet flows divide corresponds to the cell length L (see Fig. 1). The cell volume V^0 is equal to $L\bar{b}w$, where $\bar{b}$ is the cell breadth. If the channel is oriented vertically (as in the experiments reported here), gravity acts in the positive z direction in the case of downward flow, and in the negative z direction for upward flow. For a high aspect ratio $\bar{b}/w$ (here 60 to 120) we can ignore the effects of the side (edge) walls on the fluid velocity profile within the cell. The regions disturbed by the drag exerted by the side walls will be a comparatively small fraction of the total cross section. The velocity profile is therefore essentially two-dimensional, provided the major walls are parallel. The mean fluid velocity $<v>$ is then equal to $\dot{V}/\bar{b}w$, and the velocity profile across the cell thickness is described by the parabolic equation

$$v\left(\frac{x}{w}\right) = 6<v>\frac{x}{w}\left(1 - \frac{x}{w}\right) = 4v_{max}\frac{x}{w}\left(1 - \frac{x}{w}\right) \tag{2}$$

where v_{max} is the maximum fluid velocity found at the midplane ($x = w/2$) of the cell. This parabolic profile is characteristic of plane Poiseuille flow.

Placement of Splitting Planes

Operation of a SPLITT cell in the transport mode requires the introduction of the sample stream as a lamina adjacent to one wall, which by convention is wall A. The separation of components, as mentioned above, is achieved by their different rates of transport toward the opposite wall (B) under the influence of the transverse field. The ratio of sample flow rate $\dot{V}(a')$ to the total flow rate $\dot{V}$ required to position the inlet splitting plane (ISP) at a distance $w_{a'}$ from wall A is given by (5, 9)

$$\frac{\dot{V}(a')}{\dot{V}} = 3\frac{w_{a'}^2}{w^2} - 2\frac{w_{a'}^3}{w^3} \tag{3}$$

The feed stream is then confined to the lamina of thickness $w_{a'}$ between wall A and the ISP (see Fig. 1). The outlet splitting plane (OSP) may be

placed at any distance w_a ($\leq w$) from wall A by withdrawing a flow rate $\dot{V}(a)$ ($\leq \dot{V}$) from outlet a. The transport zone extends from the ISP to the OSP and has a thickness $w_t = w_a - w_{a'}$. It has been shown (4) that when the driving force across the cell thickness is constant (and perturbations to particle friction factors and velocity, caused by the presence of the walls, are ignored), the precise cell thickness and the positions of the splitting planes need not be known in order to predict the fraction of each component exiting either outlet. In this case the fraction of a sample component retrieved at each outlet may be predicted knowing only the volumetric inlet and outlet flow rates, the transverse migration velocity of the sample component, and the cell area $L\bar{b}$. When the driving force is position-dependent however, the fraction of each component collected at each outlet will not be independent of the placement of the splitting planes. The hydrodynamic lift forces utilized in the present study are strongly position-dependent as we shall describe below.

Hydrodynamic Lift Forces

These were discussed in some detail in an earlier publication (10). For a small spherical particle entrained in plane Poiseuille flow between parallel bounding walls, fluid inertia is predicted (11–15) to give rise to a transverse force described approximately by (10)

$$F_{Li} = F_{Li}(I) + F_{Li}(II) + F_{Li}(III) \tag{4}$$

where

$$F_{Li}(I) = 119.1\pi \frac{\nu_{max}^2 a^4 \rho}{w^2} \left(0.19 - \frac{x}{w}\right)\left(0.5 - \frac{x}{w}\right)\left(0.81 - \frac{x}{w}\right) \times \left(1 + \frac{16}{25}\frac{x}{w}\left(1 - \frac{x}{w}\right)\right) \tag{5}$$

$$F_{Li}(II) = -\frac{33}{4}\pi U_z \nu_{max} a^2 \rho \frac{x}{w}\left(0.5 - \frac{x}{w}\right)\left(1 - \frac{x}{w}\right)\left(1 - \frac{5}{2}\frac{x}{w}\left(1 - \frac{x}{w}\right)\right) \tag{6}$$

and

$$F_{Li}(III) = \frac{9}{8}\pi U_z^2 a^2 \rho \left(1 + \frac{x}{w} - \left(\frac{x}{w}\right)^2\right)\left(0.5 - \frac{x}{w}\right) \tag{7}$$

where ρ is the density of the fluid and U_z is the sedimentation velocity

(i.e., the Stokes velocity) of the particle in unbounded fluid in the direction of the z-axis. If the channel is oriented vertically, the unbounded sedimentation velocity is given by

$$U_z = \frac{F_z}{6\pi\eta a} = \frac{2a^2\Delta\rho G}{9\eta} \tag{8}$$

where F_z is the force on the particle due to gravity in the z direction, η is the fluid viscosity, $\Delta\rho$ is the excess density of the particle over that of the fluid, and G is the acceleration due to gravity. If $\Delta\rho$ is positive and flow is in the downward direction, then, following the convention described earlier, G, and hence F_z and U_z, will be positive. The derivation of the inertial lift force expressions required the assumption that a/w, a/x, and $a/(w - x)$ are all much smaller than unity, i.e., the particle must be small compared to the cell thickness, and it must not be close to either wall. It was also required that both the channel Reynolds number Re ($= wv_{max}\rho/\eta$) and a particle Reynolds number defined as $aU_z\rho/\eta$ be small compared to unity. It has since been shown (16, 17) that at high channel Re the inertial lift for a neutrally buoyant particle is slightly lower than predicted by Eq. (5), and the points at which $F_L = 0$ (i.e., $x/w = 0.19$ and 0.81 in Eq. 5) move closer to the walls. The general behavior is similar however.

The overall transverse force due to fluid inertial effects as shown in Eq. (4) is given as the sum of the three contributions $F_{Li}(I)$, $F_{Li}(II)$, and $F_{Li}(III)$. Under differing conditions, any one of the three may dominate, the one exception being that the second contribution $F_{Li}(II)$, which always approaches zero at the walls, may dominate across the central region but not near the walls. Under intermediate conditions a combination of either $F_{Li}(I)$ and $F_{Li}(II)$, or $F_{Li}(II)$ and $F_{Li}(III)$, will account for overall inertial lift. For the case of neutrally buoyant particles, or the case of nonneutrally buoyant particles in horizontal flow, U_z is zero and inertial lift is described by $F_{Li}(I)$ alone. A criterion for neutral buoyancy in vertical flow may be written as (13, 14)

$$|U_z| << \left(\frac{a}{w}\right)^2 v_{max} \tag{9}$$

This condition is sufficient for $F_{Li}(I)$ to dominate. Under these conditions, particles are driven toward two stable equilibrium positions at $x/w = 0.19$ and 0.81, and away from an unstable equilibrium position at $x/w = 0.5$.

For conditions giving rise to small $|U_z|$, such that Condition (9) is not satisfied, $F_{Li}(II)$ becomes significant. Due to the symmetry of the system, all contributions approach zero at the channel midplane, and as mentioned

above, $F_{Li}(II)$ approaches zero at the walls. For the intermediate regions, $F_{Li}(II)$ acts away from the walls when sedimentation is against the channel flow, and toward the walls when sedimentation is in the direction of flow. The net result is that sedimentation against the flow tends to move the equilibrium positions toward the channel midplane, while sedimentation in the direction of flow tends to move them closer to the walls.

When sedimentation velocity U_z becomes of the same order of magnitude as v_{max}, the first contribution will have become negligible, since it is required that $a/w << 1$. The third contribution $F_{Li}(III)$, however, now becomes significant. This contribution always acts away from the walls toward the midplane. With sedimentation against the flow, $F_{Li}(II)$ and $F_{Li}(III)$ act together to drive the particle toward the center. When sedimentation is in the direction of flow, the contributions oppose each other in the central regions. Near the walls there will always be a net force toward the channel center, but when $U_z \approx v_{max}/2$ the two contributions effectively cancel over the range of x/w from 0.15 to 0.85 (see Ref. 10). Under such conditions there is negligible net force across this central region due to fluid inertia. For still higher U_z, or for the case of quiescent fluid where $v_{max} = 0$, $F_{Li}(III)$ describes overall lift. In this case the inertial force drives particles away from the walls toward the channel center.

The particle separation technique of field-flow fractionation (FFF) (18, 19), in common with SPLITT fractionation, is carried out within thin parallel plate channels. In the steric and steric-hyperlayer modes of operation (20–23), each particle size is driven to a specific equilibrium position within the parabolic carrier velocity profile, and so migrates along the length of the system at a specific velocity. Separation of different sized particles is achieved by way of their differing equilibrium positions and hence their differing longitudinal velocities. The equilibrium position of a particle is the point of balance; here the force on the particle due to an applied transverse field equals the opposing lift forces. Measurement of a particle's velocity, via its elution time through the system, allows the determination of its equilibrium position. This in turn provides a precise measure of the lift force at this position since it must be equal but opposite to the force generated by the applied field, the strength of which is known. Experiments (24–26) have determined that near the walls the lift force on rigid spherical particles may greatly exceed that predicted by Eq. (5). The excess contribution to lift from a single wall was shown to be described by

$$F_{Lw} = C\frac{a^3\eta s_0}{\delta} = \frac{6Ca^3\eta<v>}{w\delta} = \frac{4Ca^3\eta v_{max}}{w\delta} \tag{10}$$

where C is a dimensionless coefficient that has some system dependence

that is not yet fully characterized, s_0 is the shear rate of the carrier at the wall, and δ is the gap distance between the particle and the wall and is equal to $(x - a)$. For the range of δ studied, a simple inverse dependence on δ was found for this contribution to lift. Experimentally determined lift was found to far exceed that predicted by Eq. (5) when the particle was close to the wall. We can account for this additional lift in a parallel plate system by summing the contributions due to the two walls as follows:

$$F_{Lw} = \frac{6Ca^3\eta<v>}{w}\left(\frac{1}{(w - a)} - \frac{1}{(w - x - a)}\right) \tag{11}$$

Restrictions on Splitting Plane Positions and Flow Rates

From the above discussion we see that nonneutrally buoyant particles, for which $0 < U_z < 0.5v_{max}$ and the inequality of Eq. (9) is not satisfied, are driven toward equilibrium points symmetrically located at $x/w < 0.19$ and > 0.81. All other conditions will lead to the driving of particles toward two symmetrically located equilibrium points at $x/w \leq 0.19$ and ≥ 0.81, or toward a single equilibrium point at $x/w = 0.5$. Operation of a SPLITT cell in the transport mode requires the net force to act continuously and monotonically throughout the region that includes the feed lamina and the OSP. In fact, the force must remain significant for some distance beyond the OSP to selectively carry some of the feed components into the laminae that exit at the *b* outlet.

In the interests of high throughput, conditions for which $0 < U_z < 0.5v_{max}$ and the inequality of Eq. (9) is not satisfied must be avoided. Consideration of all other possible conditions shows that in the worst case, again from the standpoint of throughput, the equilibrium position would be located at $x/w = 0.19$. The OSP would have to be placed between $x = 0$ and this point, and the ISP between $x = 0$ and the OSP to obtain a thin transport zone. Thus

$$0 < \frac{w_{a'}}{\mathrm{w}} < \frac{w_a}{w} < 0.19 \tag{12}$$

(In some cases the middle inequality may not be necessary because lift forces in the inlet region would force incoming particles away from the ISP and thus create an effective transport zone where none would otherwise exist.)

From Eq. (3) we see that Eq. (12) places the following restriction on flow rates:

$$0 < \frac{\dot{V}(a')}{\dot{V}} < \frac{\dot{V}(a)}{\dot{V}} < 0.0946 \tag{13}$$

This restriction is undesirable because throughput is proportional to $\dot{V}(a')$, which is strongly limited.

The best case would result from an equilibrium position at $x/w = 0.5$, which would be expected either when $(-U_z/v_{max})(w/a)^2 > 15$ or when conditions generate sufficiently high near-wall contributions to lift. In this situation it would be required that

$$0 < \frac{w_{a'}}{w} < \frac{w_a}{w} < 0.5 \tag{14}$$

so that the less restrictive conditions on volumetric flow rates are given by

$$0 < \frac{\dot{V}(a')}{\dot{V}} < \frac{\dot{V}(a)}{\dot{V}} < 0.5 \tag{15}$$

In practice, the positioning of the splitting planes closer to wall A might aid the speed of separation by making use of the stronger lift forces that operate close to the wall.

Particle Friction Coefficients and Wall Effects

As explained in our earlier publication (10), a particle that is subjected to a force moves relative to the surrounding fluid but at a velocity that is perturbed by the presence of bounding walls. If bounding walls are relatively far from the particle, its velocity v_p will be close to that predicted by the Stokes–Einstein equation:

$$v_p = \frac{F}{f} = \frac{F}{6\pi\eta a} \tag{16}$$

where f is the particle friction coefficient. When the particle is close to a bounding wall the velocity will be reduced, the reduction represented by a perturbation in the particle friction coefficient. Multiplicative correction factors to f have been obtained for migration of a spherical particle perpendicular to (27–33) and parallel to (34–38) plane bounding walls. For the coordinate system of our SPLITT cell these factors are given the symbols Γ_x and Γ_z, respectively. These correction factors generally require numerical solution, but reduce to simple analytical expressions at the limits corresponding to close proximity to a wall, and at the other extreme, to removal from the vicinity of a wall. We have discussed the accuracy of these expressions and have proposed methods for obtaining good approximations to Γ_x and Γ_z for a particle situated at any point within a parallel plate system (10).

The determination of the forces and torques on both an oblate and a prolate spheroid, and on a torus and a biconcave disk, entrained in shear flow near a wall has been reported (39). The latter corresponds to the shape of an undeformed human red blood cell and is of direct relevance to some of the experiments reported below. It was shown that when the particle is not very close to the wall, an oblate spheroid closely approximates the behavior of a biconcave disk. The results are dependent on the orientation of the axis of symmetry relative to the wall however, and the resultant motion of a continuously tumbling particle is therefore complicated. The theory for this tumbling motion has been studied and recently published (40).

Retardation of Particle in Bounded Shear Flow

Goldman, Cox, and Brenner (41) showed that the velocity of a neutrally buoyant particle entrained in shear flow adjacent to a plane wall will be smaller than the undisturbed fluid velocity at the position of the particle center. The ratio of particle velocity to this undisturbed fluid velocity was shown to be a function of δ/a or of x/a. We have referred to this ratio in our earlier publications (10, 24) as the *particle retardation factor*, and here we shall assign it the symbol **f**. The retardation factor has been determined for plane Poiseuille flow between parallel walls (37, 38). We have discussed previously (10) the accuracy of limiting analytical expressions and proposed a method for obtaining a good estimate for the factor for parallel plate systems.

Determination of Particle Trajectory

The method of trajectory determination has been described previously (10). The complicated dependence of Γ_x, Γ_z, **f**, and v on x/w is taken into account by assuming particle velocity in x and z coordinates remains constant over small time intervals δt. The corresponding increments δx and δz are summed to obtain the trajectory. The local component of particle velocity in the x coordinate v_{px} is given by

$$v_{px} = \frac{F_L}{6\pi\eta a\Gamma_x} \tag{17}$$

where F_L is the local strength of the lift force given by the sum of Eqs. (4) and (11), and Γ_x is the local correction to particle friction factor for migration perpendicular to the walls. The local component of particle velocity in the z coordinate for a nonneutrally buoyant particle entrained in

vertical plane Poiseuille flow is given by

$$v_{pz} = \mathbf{f}\cdot v(x/w) + \frac{F_z}{6\pi\eta a\Gamma_z} = \mathbf{f}\cdot v(x/w) + \frac{2a^2\Delta\rho G}{9\eta\Gamma_z} \tag{18}$$

We can set a basic time interval δt according to

$$\delta t = \frac{L}{<v> N_t} = \frac{V^0}{\dot{V}N_t} \tag{19}$$

where N_t corresponds to some arbitrary number of time intervals for migration along the full length L of the cell at the mean fluid velocity $<v>$. It follows that the distance migrated in this time interval by a particle in the x direction is given by

$$\delta x = v_{px}\delta t = \frac{F_L \quad V^0}{6\pi\eta a\Gamma_x \dot{V}N_t} \tag{20}$$

and the distance migrated along the cell length in this time is given by

$$\delta z = v_{pz}\delta t = 6\frac{\mathbf{f}}{N_t}\frac{x}{w}\left(1 - \frac{x}{w}\right)L + \frac{2a^2\Delta\rho G V^0}{9N_t\eta\Gamma_z\dot{V}} \tag{21}$$

In practice, the δt are subdivided when necessary to confine δx to some limiting fraction of a in the regions close to the walls, and elsewhere to some limiting fraction of w. The complicated dependence of F_L, Γ_x, Γ_z, and $\mathbf{f}$ on x/w precludes the determination of any simple dependence of migration distance across the channel thickness on L, $<v>$, or w. We can, however, draw some broad conclusions for neutrally buoyant particles that are confined to the region of influence of a single wall. In this case the lift force is assumed to be described as the sum of $F_{Li}(I)$ given by Eq. (5) and F_{Lw} given by Eq. (10). It can then be shown that

$$\frac{La^2}{6\pi w^3} = \int_{x_1/w}^{x_2/w} \frac{\Gamma_x \mathbf{f}\xi(1 - \xi)(\xi - a/w)}{(9/4)\pi<v>a(\rho/\eta)(\xi - a/w)g(\xi) + C}\, d\xi \tag{22}$$

where the variable of integration ξ represents x/w, and $g(\xi)$ is given by

$$g(\xi) = 19.85(0.19 - \xi)(0.5 - \xi)(0.81 - \xi)\left(1 + \frac{16}{25}\xi(1 - \xi)\right) \tag{23}$$

The integration in Eq. (22) is carried out over a range from an initial fractional distance across the channel x_1/w to a final fractional distance x_2/w attained at a point just preceding the outlet splitter. From Eq. (22) we see that if the inertial contribution to lift dominates throughout the

migration, then, for a given a and x_1/w, it follows that x_2/w increases with increase of L, ρ/η, and $<v>$, and increases more strongly with reduction of w. If the near-wall contribution to lift dominates, then once again x_2/w increases with increase of L, and increases more strongly with reduction of w, but in this case x_2/w is independent of $<v>$.

COMPUTER SIMULATIONS

The program to determine particle trajectories has already been described (10). The other programs described here were based upon sets of representative particle trajectories determined for each discrete particle size. It was assumed that particle concentration was sufficiently low that particle–particle interactions were negligible.

A program was written to consider a fixed flow regime and to calculate the fractional retrieval of material at each outlet as a function of particle size. To carry out this procedure, the size range of particles was divided into a set of discrete sizes. Each of these discrete sizes was then represented by a set of trajectories starting at equally spaced transverse positions on the sample side of the ISP (allowing for steric exclusion as explained in Ref. 10). Use was made of the fact that if, for a given particle size, the trajectory starting closest to wall A crosses the OSP, then all other trajectories must also do so, in which case the fractional retrieval at outlet b is unity, $F_b = 1$. Similarly, if the trajectory starting closest to the ISP does not cross the OSP, then $F_a = 1$. Only for a small range of particle diameter $d\ (= 2a)$ is it necessary to determine the distribution of particles on each side of the OSP close to the outlet splitter. Another program was written to carry out a determination of particle trajectories for a set of discrete particle sizes with both $\dot{V}(a')$ and $\dot{V}$ fixed. For each particle size the fractional retrieval at each outlet is determined as a function of $\dot{V}(a)/\dot{V}$. A third program determines fractional recoveries for a given particle size as a function of mean flow velocity $<v>$ while the flow ratios $\dot{V}(a')/\dot{V}$ and $\dot{V}(a)/\dot{V}$ are held constant.

For all three programs the calculations could be weighted either for a pulse or for continuous sample input. For the case of continuous sample input, the trajectories are weighted according to the carrier velocity at their starting points. This accounts for the differing sample input flux represented by each trajectory. This weighting influences the fractional retrieval of those components that are distributed between the two outlets. The effect of the different weightings is illustrated by consideration of a simple gravitational SPLITT system (4), where particle size effects, lift forces, and velocity perturbations are ignored. For continuous operation

it can be shown that (4)

$$F_a = \frac{\dot{V}(a)}{\dot{V}(a')} - \frac{\Delta\dot{V}}{\dot{V}(a')} \tag{24}$$

provided $\dot{V}(a) - \dot{V}(a') \leq \Delta\dot{V} \leq \dot{V}(a)$, where $\Delta\dot{V} = \bar{b}LU_x$ in which U_x is the constant migration velocity in the x direction. We see that F_a is predicted to vary linearly with $\dot{V}(a)$. At the other extreme is a pulse input, in which a narrow pulse of particles in the inlet region of the SPLITT cell is allowed to equilibrate and thus reach a uniform concentration across all streamlines just prior to being swept beyond the edge of the inlet splitter. For such a pulse input it may be shown that

$$F_a = \frac{w}{w_{a'}}(\sin(\phi/3) + 0.5) \tag{25}$$

where

$$\sin(\phi) = \frac{2(\dot{V}(a) - \Delta\dot{V})}{\dot{V}} - 1 \tag{26}$$

with ϕ confined to the range $-\pi/2 < \phi \leq \pi/2$, and where again $\dot{V}(a) - \dot{V}(a') \leq \Delta\dot{V} \leq \dot{V}(a)$. For pulse input we see that F_a does not vary linearly with $\dot{V}(a)$. In reality, neither the continuous nor pulse inputs will provide a highly accurate representation of particle distributions prior to the entry of particles into the active fractionation region of the SPLITT cell. Lift forces in the entry region of the cell (adjacent to the inlet splitter) will drive particles away from the outer boundaries of the inlet lamina. This will tend to bias the initial distribution more toward that assumed for a continuous input regardless of the actual input conditions. All of the calculations reported here are for pulse input conditions. However, as we will show later, the separation process is not very sensitive to initial conditions because, under the influence of hydrodynamic lift forces, all trajectories for particles of a given size tend to converge into a narrow region of the SPLITT cell despite significant differences in their initial positions (see Fig. 9).

For continuous sample input, the programs determine the outlet stream concentrations (relative to input concentration) as functions of d for fixed $\dot{V}(a')$, $\dot{V}(a)$, and $\dot{V}$; as functions of $\dot{V}(a)/\dot{V}$ for fixed $\dot{V}(a')$, $\dot{V}$, and d; and as functions of $<v>$ for fixed $\dot{V}(a')/\dot{V}$, $\dot{V}(a)/\dot{V}$, and d; respectively.

EXPERIMENTAL

The general construction of a SPLITT cell has been described previously (4). Each cell used in this work was constructed using two Mylar

spacers, separated by either a stainless steel layer or another Mylar layer out of which the rectangular cell outline was cut. Longer rectangular outlines (of the same breadth $\bar{b}$) were cut from the Mylar spacers. These outlines were tapered toward the inlets and outlets bored through the glass plates forming the cell walls and through the Plexiglas blocks used to hold the system together. The excised outlines were aligned with each other and with the inlets and outlets before bolting the system together. The stainless steel or Mylar center layer at each end of the removed rectangular section served as the inlet and outlet splitters. The condition of the splitters is of great importance. The edges must be straight without deformities that would interfere with the flowing streams. They must not bow or buckle when clamped in the system. To assure uniformity, the outer margins of the splitter layer, at points in line with the splitter edges, were held by external clamps. Outward force of the clamps, exerted via grub screws, held the splitters taut. The use of high $\dot{V}(b')/\dot{V}(a')$ ratios results in a lateral pressure on the splitter that increases with $\dot{V}$. The tension in the splitters tends to reduce any resulting deflection.

Four SPLITT cells were used in this work. Three were constructed with Mylar spacers of thickness 102 μm and stainless steel splitters of thickness 127 μm, giving a total thickness of 330 μm. Two cells, of length 2 and 10 cm (measured between the splitter edges), each had a breadth of 2 cm. A 30-cm long cell was constructed with a breadth of 4 cm. In addition, a cell of reduced thickness (230 μm) was constructed of three 76 μm layers of Mylar. This cell had a length of 10 cm and a breadth of 2 cm.

The channels were mounted vertically with flow in the downward direction. Two pumps provided independent flow streams to the inlets a' and b'; a Cheminert metering pump (Chromatronix, Berkeley, California) for inlet a' and a Kontron LC414 pump (Kontron Electrolab, London, United Kingdom) for inlet b'. A second Cheminert pump was modified to operate smoothly in reverse as a suction pump, or "unpump," to control the flow from outlet a. The flow at outlet b was then governed by mass conservation.

An Altex 153 UV absorbance detector (Altex, Berkeley, California) and a Spectroflow 757 absorbance detector (Kratos, Ramsey, New Jersey), operated at a wavelength of 254 nm, were used to monitor particle concentration at outlets a and b, respectively. Connection of the detectors in series allowed the determination of their relative response. A dual channel chart recorder (Omniscribe, Houston, Texas) was used to record detector signals.

Although SPLITT systems do have the capacity for continuous mode operation, samples were introduced into flow stream a' using an injection

valve (Valco, Houston, Texas) equipped with a 0.10-mL loop. This method is ideal for the investigative work reported here. It minimizes the run time and conserves sample materials.

The carrier fluid for the latex bead samples was composed of 0.1% (v/v) FL-70 (a commercial surfactant supplied by Fisher Scientific, Fair Lawn, New Jersey) and 0.02% (w/v) sodium azide as a bactericide (Sigma Chemicals, St. Louis, Missouri) in doubly distilled, deionized water. The FL-70 served to stabilize the sample suspensions and to help keep the system free of bubbles. For red blood cell (RBC) and bovine serum albumin (BSA) samples, the carrier was a 0.1 M phosphate buffer (pH 7.3 to 7.4) made up in the same purified water.

Monodisperse polystyrene divinylbenzene latex bead standards (Duke Scientific, Palo Alto, California) (referred to here as PSB) in the 2 to 50 μm diameter range were injected as supplied for the initial experiments. For later experiments the supplied suspensions were centrifuged and resuspended in carrier solution three times before use to remove low molecular weight impurities. These impurities were found to absorb at 254 nm and thereby interfere with the calculation of particle retrieval at each outlet. Sample concentrations were estimated to be ~1% by weight. Human RBC samples were obtained from one of the authors (J.Z.) and fish RBC samples from freshly killed grass carp. In each case the whole blood samples were diluted by the buffered carrier (2 drops per 6 mL of carrier). BSA was obtained from Sigma Chemicals (St. Louis, Missouri) and made up to 0.05% (w/v) in the buffered carrier.

For the experiments involving the separation of binary mixtures of PSB samples or of RBC from serum, the liquid exiting from each outlet was collected, concentrated by centrifugation, and subjected to direct particle counting using a Bright-Line hemacytometer counting chamber (AO Scientific Instruments, Buffalo, New York). The presence of different sized PSB in a collected fraction was easily observed, and the counting of each particle size was made without difficulty in the presence of the other.

RESULTS AND DISCUSSION

Fractionation of PSB

These experiments were carried out using the SPLITT cells of thickness 330 μm, breadth 2 cm, and lengths of 2 and 10 cm. All experiments were carried out using $\dot{V}(a') = 0.20$ mL/min, and $\dot{V}(b') = 8.0$ mL/min, so that $\langle v \rangle = 2.07$ cm/s. The relative sample lamina thickness $w_{a'}/w$ is calculated (5) using the equation

$$w_{a'}/w = \sin(\theta/3) + 0.5 \tag{27}$$

where

$$\sin(\theta) = 2\frac{\dot{V}(a')}{\dot{V}} - 1 \tag{28}$$

with θ confined to the range $-\pi/2 < \theta \leq \pi/2$. It follows that $w_{a'}/w = 0.093$.

Assuming vertical orientation of the channel, for which U_z is given by Eq. (8), the criterion for neutral particle buoyancy (Eq. 9) reduces to

$$\left|\frac{4w^2\Delta\rho G}{27\eta\langle v\rangle}\right| << 1 \tag{29}$$

We find that for PSB ($\Delta\rho = 0.05$ g/mL), the left-hand side of the required inequality above is 0.43 for the experimental conditions used (assuming $G = 981$ cm/s^2 and $\eta = 0.0089$ poise at 298 K). The inequality is therefore not strongly fulfilled.

Samples of the supplied suspensions of 2, 10, 20, 30, and 50 μm PSB were introduced individually into the 2-cm long cell at the fixed $\dot{V}(a')$ and $\dot{V}(b')$ reported above. Detector signals were recorded for each sample for a range of discrete $\dot{V}(a)/\dot{V}$ values. The fraction of a sample retrieved at outlet b was calculated by

$$F_b = \frac{A_b\dot{V}(b)}{R_{b/a}A_a\dot{V}(a) + A_b\dot{V}(b)} \tag{30}$$

where F_b is the fractional retrieval at b, and A_a and A_b are the areas under the peaks recorded for outlets a and b, respectively. The response ratio $R_{b/a}$ is the ratio of the response at detector b to that at detector a when they are connected in series.

The results obtained for the 2-cm long cell are plotted in Fig. 2 as F_b vs $\dot{V}(a)/\dot{V}$ for each particle size. The plots clearly demonstrate the increase in the lift-induced transverse particle velocity with increasing particle size. Half of the 50 μm particles are retrieved at outlet b when $\dot{V}(a)/\dot{V} = 0.10$; this implies that half of the 50 μm particles are driven across the outlet splitting plane at $w_a/w = 0.20$. By contrast, an outlet splitting ratio corresponding to $\dot{V}(a)/\dot{V} \approx 0.05$ results in $F_b \approx 0.5$ for 30 μm particles, indicating that half the 30 μm particles are driven across the OSP at $w_a/w = 0.14$. Smaller particles have lower transverse (lift-driven) migration velocities and their F_b values are therefore lower at any given $\dot{V}(a)/\dot{V}$.

It is also seen from Fig. 2 that $F_b < 0.9$ for even the 50 μm particles at all $\dot{V}(a)/\dot{V}$. This suggests either some imperfection in the outlet splitter of this system or the presence of low molecular weight impurities in the sample suspensions. The latter possibility was confirmed by sedimenting

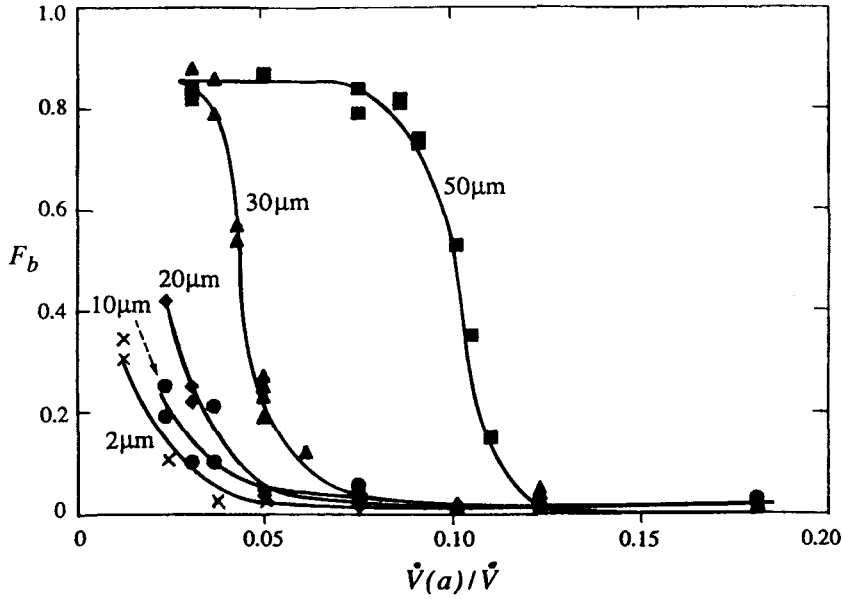

FIG. 2 Experimentally determined fractional retrieval of 2, 10, 20, 30, and 50 μm polystyrene divinylbenzene particles at b outlet of 2-cm long cell, with variation of $\dot{V}(a)/\dot{V}$. For all experiments $\dot{V}(a') = 0.2$ mL/min and $\dot{V}(b') = 8.0$ mL/min.

the particulate samples and resuspending them in carrier, as described earlier. The resultant suspensions did not exhibit the limited range of F_b. The washed samples were used for all later experiments.

It is apparent from Fig. 2 that this 2-cm long system could be used to separate 50 and 30 μm particles. For $\dot{V}(a)/\dot{V} = 0.075$ the plots suggest that >80% of the 50-μm particles would be collected at outlet b and >95% of the 30-μm particles at outlet a. Figure 3 shows photomicrographs of a feed mixture of 30 and 50 μm particles (3.4:1 by number) and of fractions collected at each outlet when $\dot{V}(a)/\dot{V} = 0.078$. The separation is seen to be excellent. Particle counting showed 99% purity (by number) for the 30-μm particles exiting at outlet a, and 94% purity for the 50-μm particles at b. The performance is better than suggested by Fig. 2 because the process of particle counting is not perturbed by the presence of the low molecular weight impurities.

The speed of particle separation within the SPLITT cell is remarkable. High separation speeds are possible because the transverse migration distances involved are so small. For the flow conditions used in the separation described above, $w_{a'} = 31$ μm and $w_a = 57$ μm. A 50-μm particle

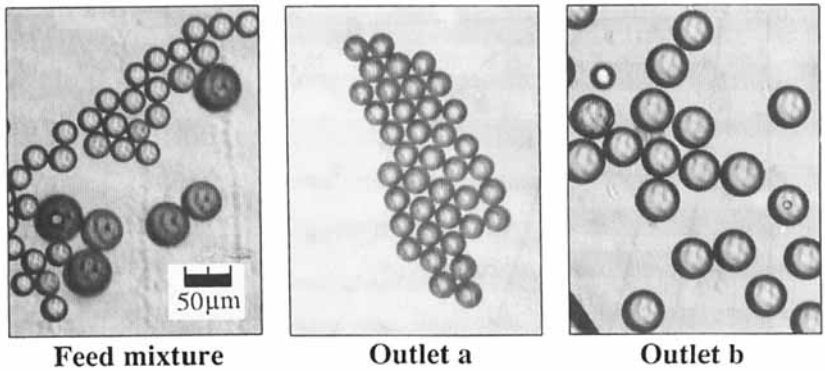

FIG. 3 Photomicrographs of feed mixture of 30 and 50 μm polystyrene divinylbenzene particles, and of fractions collected at *a* and *b* outlets of 2-cm long cell.

that starts its migration adjacent to wall A must be deflected only ~32 μm toward wall B as it is carried through the cell. For complete separation a 30-μm particle that starts its migration from just within the ISP must not have time to be deflected more than 41 μm toward wall B. The carrier flow velocity at the position of the ISP is 0.49 cm/s, so that an element of fluid on the ISP passes through the cell in 4.1 seconds. The particle separation is achieved in a comparable time.

Results obtained for the washed samples with the 10-cm long cell are shown in Fig. 4. We note that the F_b curves are displaced toward higher $\dot{V}(a)/\dot{V}$ due to the greater residence time and thus the longer time available for transverse migration within the longer cell. The increased transverse migration is also expected, as mentioned earlier, from consideration of Eq. (22). We also see from Fig. 4 that for each particle size, F_b varies over the full range from 1 to 0 with increase of $\dot{V}(a)/\dot{V}$, this improvement being due to the sample pretreatment described. We observe that whereas 30 and 50 μm particles could be separated with the 2-cm cell, this is not possible with the 10-cm cell. This is partly due to the F_b curves being closer to one another and partly due to the less abrupt fall in F_b with increase in $\dot{V}(a)/\dot{V}$ for each particle size. The longer time for transverse migration does, however, result in successful separation of 10 and 20 μm particles, a separation that was impossible with the shorter cell. Photomicrographs of a feed mixture of 10 and 20 μm particles (2.6:1 by number) and of collected fractions at the two outlets for $\dot{V}(a)/\dot{V} = 0.049$ are shown in Fig. 5. Particle counting showed 98% purity (by number) for the 10-μm particles and between 70 and 90% purity for the 20-μm particles (the latter range reflects the experimental irreproducibility).

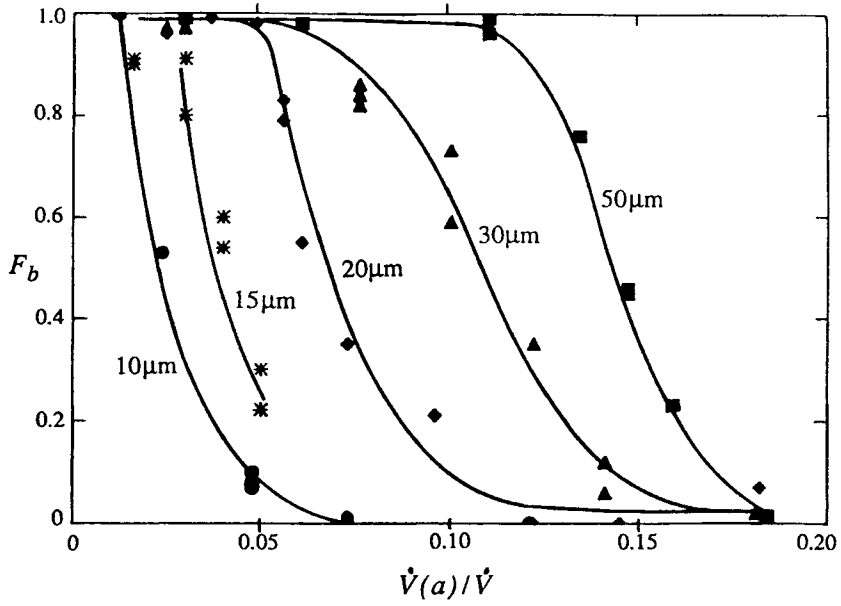

FIG. 4 Experimentally determined fractional retrieval of 10, 15, 20, 30, and 50 μm polystyrene divinylbenzene particles at *b* outlet of 10-cm long cell, with variation of $\dot{V}(a)/\dot{V}$. For all experiments $\dot{V}(a') = 0.2$ mL/min and $\dot{V}(b') = 8.0$ mL/min.

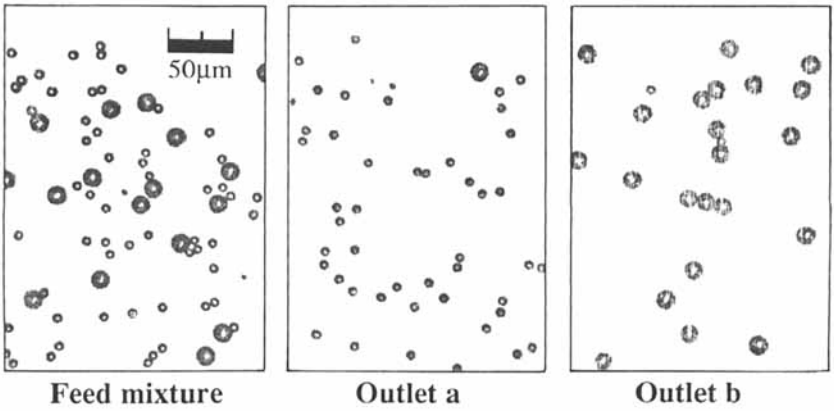

FIG. 5 Photomicrographs of feed mixture of 10 and 20 μm polystyrene divinylbenzene particles, and of fractions collected at *a* and *b* outlets of 10-cm long cell.

Figures 6 and 7 show predicted F_b vs $\dot{V}(a)/\dot{V}$ curves for the 2- and 10-cm cells, respectively, at the conditions used in the experiments. The results were calculated for pulse input, and the effects of gravity in the direction of flow were taken into account. As expected, the effects of gravity were small. The value assumed for the coefficient C (of Eq. 11) had a much greater effect. The inertial contributions to lift were not sufficient to account for the transverse migration distances indirectly observed through measurement of F_b. The contribution of an additional force such as provided by Eq. (11) was necessary. A value of 0.06 for C was found to give a reasonable match with experiment. This compares to values found via steric FFF measurements (24, 25) which ranged from about 0.005 to 0.15 for different systems. The predicted F_b is seen to drop rapidly from 1 to 0 over a small range of $\dot{V}(a)/\dot{V}$ for each particle size, far more rapidly than observed in the reported experiments. The discrepancy may be due to a number of factors, such as imperfections in the splitters, influence of the side walls on the motion of the particles near the edges, particle motion in the transition regions close to the splitters, and, to a lesser extent, sample polydispersity.

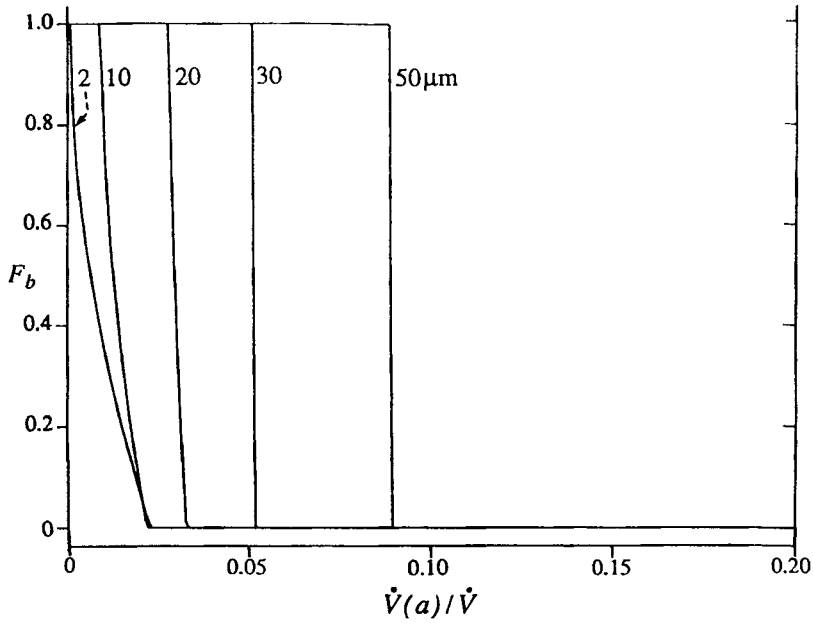

FIG. 6 Predicted fractional retrieval of 2, 10, 20, 30, and 50 μm polystyrene divinylbenzene particles at outlet b of 2-cm long cell. Experimental conditions as for Fig. 2.

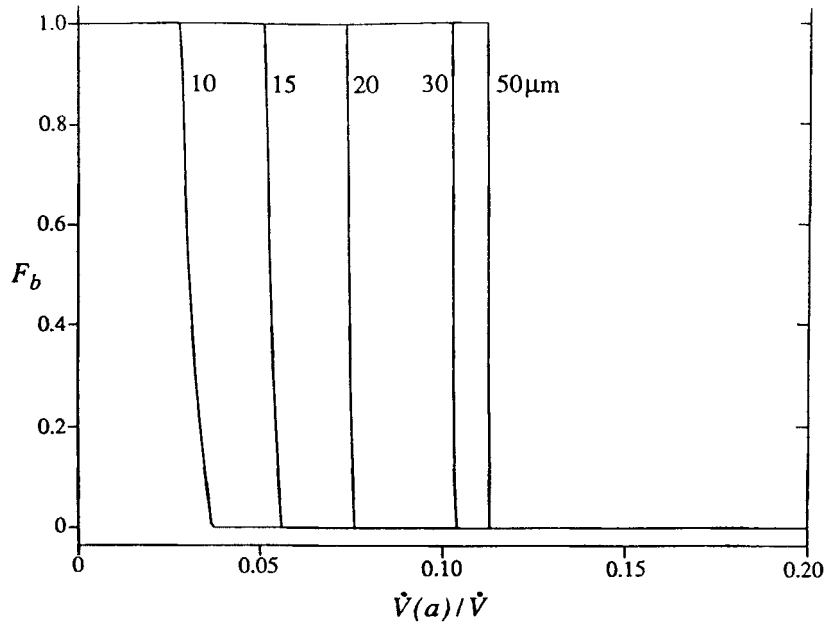

FIG. 7 Predicted fractional retrieval of 10, 15, 20, 30, and 50 μm polystyrene divinylbenzene particles at outlet b of 10-cm long cell. Experimental conditions as for Fig. 4.

The predictions of Figs. 6 and 7 suggest a potential for fractionating material at extremely sharp cutoffs. Figure 8 shows the predicted variation of F_b with d for the 10-cm cell with $\dot{V}(a') = 0.2$ mL/min, $\dot{V}(b') = 8.0$ mL/min, and $\dot{V}(a)/\dot{V} = 0.049$. The predicted sharp cutoff (with a spread of only ~1 μm) is the result of an effective focusing of particles of similar size. This occurs because the particles initially located close to wall A experience stronger lift forces than those further away. This effect continues to operate during migration through the system, forcing similar-sized particles into an increasingly confined region of the channel thickness. This is illustrated in Fig. 9 by the trajectories generated for 13, 14, and 15 μm particles under conditions corresponding to those for Fig. 8. None of the 13-μm particles are predicted to cross the OSP, while all of the 15-μm particles are predicted to do so.

Separation of RBC from Serum

Human RBCs are biconcave disk-shaped particles. They are both polydisperse in size and nonrigid. They have a mean diameter of around 8 μm and a thickness of ~2 μm (e.g., Ref. 42). They are also not uniform in

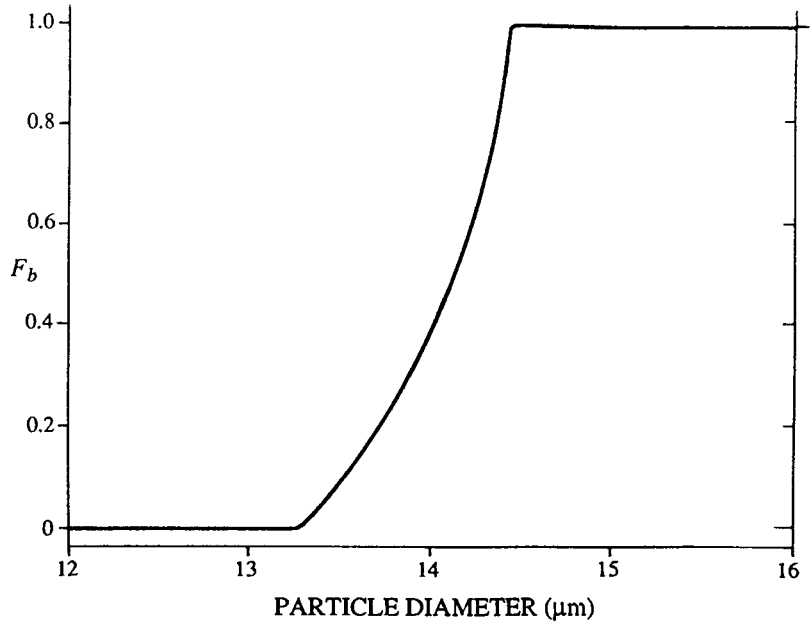

FIG. 8 Predicted fractional retrieval at outlet b of 10-cm long cell as a function of particle diameter. Experimental conditions assumed: $\dot{V}(a') = 0.2$, $\dot{V}(b') = 8.0$ mL/min, and $\dot{V}(a)/\dot{V} = 0.049$, with particle density corresponding to polystyrene divinylbenzene.

density, averaging 1.10 to 1.11 g/mL (43). It is not reasonable to expect the theory developed for rigid spherical particles to apply, without modification, to their motion. We can, however, compare their behavior to that of PSBs. The grass carp RBC are oblate spheroids with a maximum diameter of ~14 μm and a minimum diameter of ~10 μm.

The objective of this work was to examine the feasibility of using hydrodynamic lift forces alone to separate red blood cells from serum which contains mostly smaller species such as proteins and salts. These smaller entities are relatively unaffected by lift forces but tend to migrate by a diffusive mechanism. It was therefore necessary to search for conditions where lift forces were able to drive a large fraction of the RBCs across the transport zone while at the same time minimizing the diffusive transport of proteins.

Because lift forces are strongest near the walls, it is important that the sample lamina and transport zone are both relatively thin in order to take advantage of the fastest possible transverse migration velocities for RBCs. There are practical limits to this requirement however. The thinner the

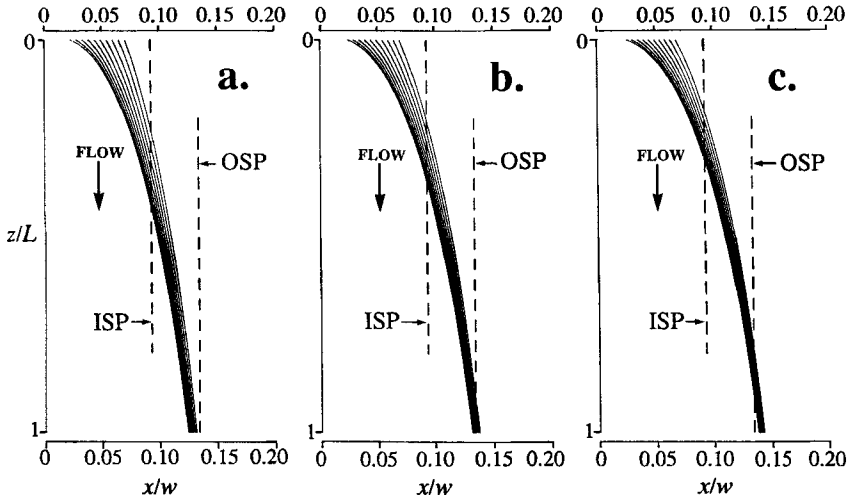

FIG. 9 Set of representative particle trajectories for (a) 13, (b) 14, and (c) 15 μm particles under conditions assumed for Fig. 8. The carrier flow and particle trajectories are in the downward direction. Inlet and outlet splitting planes (ISP and OSP, respectively) are represented by vertical dashed lines.

sample lamina (for a given $\dot{V}$), the lower will be the sample throughput. Also, as the thickness of the sample lamina and transport zones are reduced, the separation is likely to become more sensitive to splitter imperfections.

Equation (22) shows that for a neutrally buoyant particle of given size the distance of transverse migration relative to cell thickness is a function of L/w^3 or of $L<v>/w^3$, depending on the dominant contribution to lift force. It has been shown (5) that for a given protein the transverse migration due to diffusion is dependent on $L/<v>w^2$. The length of the cell must be sufficient for a large fraction of the RBC to migrate across the transport zone, and the required L will therefore be dependent on the placement of the splitting planes and thus the transport zone. However, beyond a certain length, a further increase in L will not improve the separation because lift-driven transport gradually attenuates while diffusive transport continues to increase. An increase in $<v>$ should enhance RBC transport and at the same time reduce protein transport. Again there may be practical limitations in that increased flow will eventually disrupt the splitting planes. Finally, a reduction in cell thickness should increase transport of RBC relative to the protein.

The fractional retrieval F_b of human RBC was measured for both the 10- and 30-cm SPLITT cells having $w = 330$ μm for a range of $<v>$ from around 2 to 8 cm/s and $\dot{V}(a')/\dot{V} = \dot{V}(a)/\dot{V} \approx 0.024$. The 10 cm-cell was found to be too short to obtain a good retrieval of RBC at the b outlet. The 30-cm cell yielded F_b of around 0.9 for RBC at $<v>$ close to 4 cm/s. Figure 10 shows the observed F_b for human RBC in the 30-cm cell with variation of $\dot{V}(a)/\dot{V}$, with the inlet split ratio $\dot{V}(a')/\dot{V}$ held at 0.030 and $<v>$ held at close to 4 cm/s. Also included in the figure is the theoretical curve for a model protein [BSA, for which the diffusion coefficient has been measured using a SPLITT system as 6.21×10^{-7} cm²/s at 293 K (44)] calculated according to the method of Reference 5. It may be seen that where F_b for the human RBC is high, the retrieval of BSA remains quite high also. The experimental F_b curve for carp RBC is displaced to higher $\dot{V}(a)/\dot{V}$ relative to that for human RBC, reflecting the increased transverse transport of the larger cells. The F_b curves suggest that the two cell populations could be rapidly but incompletely fractionated under the stated conditions.

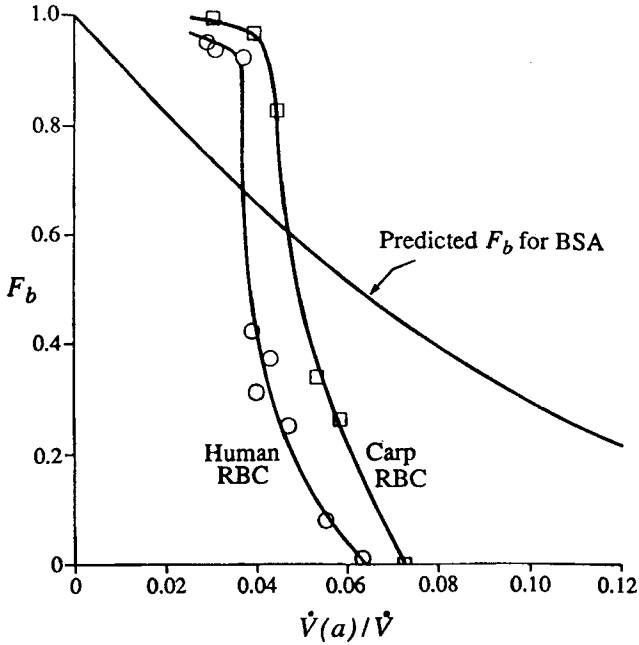

FIG. 10 Experimentally determined fractional retrieval of both human and carp red blood cells at outlet b of 30-cm long cell of thickness 330 μm, together with predicted retrieval for model protein BSA under the same conditions [$\dot{V}(a')/\dot{V} = 0.03$ and $<v> = \sim 4$ cm/s].

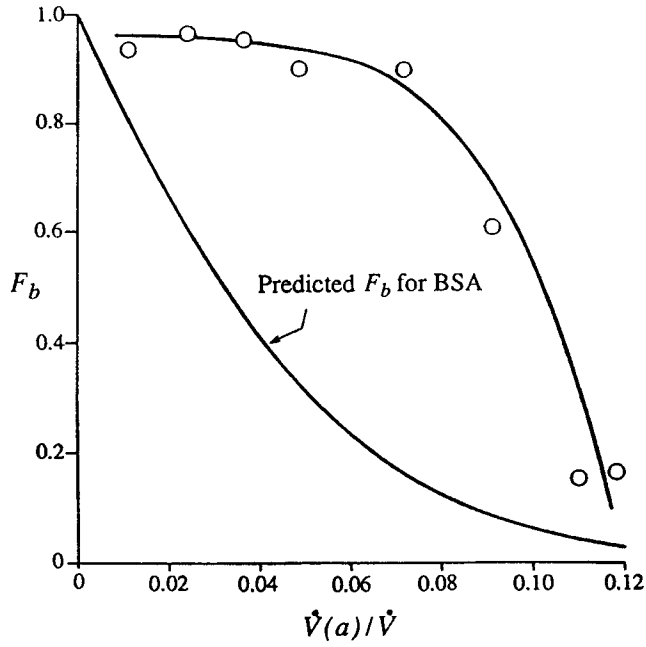

FIG. 11 Experimentally determined fractional retrieval of human red blood cells at outlet b of 10-cm long cell of reduced thickness (230 μm), together with predicted retrieval for model protein BSA under the same conditions [$\dot{V}(a')/\dot{V}$ = 0.012 and $<v>$ = 7.9 cm/s].

Finally, a channel of reduced thickness (230 μm) was examined to see if human RBC transport could be improved. The results are shown in Fig. 11. The inlet split ratio $\dot{V}(a')/\dot{V}$ was also reduced to 0.012 to utilize the region where lift forces are strongest and $<v>$ was set at 7.9 cm/s. The retrieval at outlet b is seen to be greatly improved. A large fraction of RBCs is apparently carried beyond an outlet splitting plane placed at $w_a/w = 0.17$, corresponding to $\dot{V}(a)/\dot{V} = 0.08$. Comparison with the predicted curve for BSA suggests that a reasonable separation may be possible. Some experimental studies were carried out using BSA, and quite good agreement was found between experiment and theory for moderately low channel flow rates of 2 cm/s, but at 8 cm/s agreement was poor. This could indicate a problem with the integrity of the splitters at increased flow.

CONCLUSIONS

The use of hydrodynamic lift forces for the fractionation of particulate materials has been shown in theory to have great potential. While the

experimental results have not shown the extremely high size selectivity predicted, the trends in particle retrieval at each of the SPLITT cell outlets are consistent with theory. The deviation of experiment from theory is most likely due to the critical alignment and rigidity demanded of the splitters, and the difficulty in achieving these requirements. We conclude that more work is necessary to exploit the significant potential of this SPLITT technique for the separation of cells and cell-sized particles.

NOMENCLATURE

Roman

a	particle radius
a	sample inlet adjacent to wall A of SPLITT cell
a'	outlet adjacent to wall A of SPLITT cell
A	wall of SPLITT cell at $x = 0$
A_a	area under peak recorded for outlet a
A_b	area under peak recorded for outlet b
b	outlet adjacent to wall B of SPLITT cell
b'	inlet adjacent to wall B of SPLITT cell
$\bar{b}$	breadth of channel or cell
B	wall of SPLITT cell at $x = w$
C	dimensionless coefficient of near-wall lift force Eqs. (10) and (11)
d	particle diameter
D_T	particle thermal diffusion coefficient
f	particle friction coefficient
f	correction to particle velocity [$= v_{pz}/v(x/w)$] along parallel plate system
F_a	fractional retrieval of sample at outlet a
F_b	fractional retrieval of sample at outlet b
F_L	total lift force
F_{Li}	lift force due to inertial effects
$F_{Li}(I)$	first contribution to F_{Li} given by Eq. (5)
$F_{Li}(II)$	second contribution to F_{Li} given by Eq. (6)
$F_{Li}(III)$	third contribution to F_{Li} given by Eq. (7)
F_{Lw}	near-wall lift force contribution described by Eqs. (10) and (11)
F_z	force on particle in z direction due to external field
$g(\xi)$	function of ξ given by Eq. (23)
G	acceleration due to gravity
L	length of channel or cell
N_t	number of time intervals corresponding to $L/<v>$

$R_{b/a}$	response ratio for detectors b and a
Re	channel Reynolds number ($= wv_{max}\rho/\eta$)
s_0	fluid shear rate at the wall
U_x	particle migration velocity in x direction
U_z	particle sedimentation velocity in z direction for unbounded fluid
$v(x/w)$	fluid velocity profile across thickness of channel or cell
v_{max}	maximum fluid velocity found at $x/w = 0.5$
v_p	particle velocity
v_{px}	particle velocity in x direction
v_{pz}	particle velocity in z direction
$<v>$	mean fluid velocity
V^0	channel or cell void volume
$\dot{V}$	total volumetric flow rate through channel or cell
$\dot{V}(a)$	volumetric flow rate at outlet a
$\dot{V}(a')$	volumetric flow rate at sample inlet a'
$\dot{V}(b)$	volumetric flow rate at outlet b
$\dot{V}(b')$	volumetric flow rate at inlet b'
w	thickness of channel or cell
w_a	distance from wall A to outlet splitting plane
$w_{a'}$	distance from wall A to inlet splitting plane
w_t	thickness of transport zone, i.e., distance between inlet and outlet splitting planes
x	distance measured across thickness of SPLITT cell, with origin at wall A
z	distance along flow axis measured from edge of inlet splitter

Greek

Γ_x	correction to particle friction coefficient for movement along x-coordinate of parallel plate system
Γ_z	correction to particle friction coefficient for movement along z-coordinate of parallel plate system
δ	distance between particle surface and plane wall
δt	small time interval defined by Eq. (19)
δx	distance moved by particle in x direction in time δt
δz	distance moved by particle in z direction in time δt
$\Delta\rho$	excess density of particle over that of carrier fluid
$\Delta\dot{V}$	defined as $\bar{b}LU_x$
ϕ	intermediate value appearing in Eqs. (25) and (26)
η	fluid viscosity
θ	intermediate value appearing in Eqs. (27) and (28)
ρ	fluid density
ξ	the ratio x/w

ACKNOWLEDGMENT

This work was supported by Grant CTS-9204086 from the National Science Foundation.

REFERENCES

1. J. C. Giddings, *Sep. Sci. Technol.*, *20*, 749–768 (1985).
2. J. C. Giddings, *Ibid.*, *23*, 931–943 (1988).
3. J. C. Giddings, in *Chemical Separations*, Vol. 1 (J. D. Navratil and C. J. King, Eds.), Litarvan, Denver, 1986, pp. 3–20.
4. S. R. Springston, M. N. Myers, and J. C. Giddings, *Anal. Chem.*, *59*, 344–350 (1987).
5. P. S. Williams, S. Levin, T. Lenczycki, and J. C. Giddings, *Ind. Eng. Chem. Res.*, *31*, 2172–2181 (1992).
6. S. Levin and J. C. Giddings, *J. Chem. Tech. Biotechnol.*, *50*, 43–56 (1991).
7. S. Levin, M. N. Myers, and J. C. Giddings, *Sep. Sci. Technol.*, *24*, 1245–1259 (1989).
8. C. B. Fuh, M. N. Myers, and J. C. Giddings, *Ind. Eng. Chem. Res.*, *33*, 355–362 (1994).
9. J. C. Giddings, *Sep. Sci. Technol.*, *23*, 119–131 (1988).
10. P. S. Williams, *Ibid.*, *29*, 11–45 (1994).
11. R. G. Cox and H. Brenner, *Chem. Eng. Sci.*, *23*, 147–173 (1968).
12. B. P. Ho and L. G. Leal, *J. Fluid Mech.*, *65*, 365–400 (1974).
13. P. Vasseur and R. G. Cox, *Ibid.*, *78*, 385–413 (1976).
14. R. G. Cox and S. K. Hsu, *Int. J. Multiphase Flow*, *3*, 201–222 (1977).
15. P. Vasseur and R. G. Cox, *J. Fluid Mech.*, *80*, 561–591 (1977).
16. J. A. Schonberg and E. J. Hinch, *Ibid.*, *203*, 517–524 (1989).
17. D. A. Drew, J. A. Schonberg, and G. Belfort, *Chem. Eng. Sci.*, *46*, 3219–3224 (1991).
18. J. C. Giddings, *Anal. Chem.*, *53*, 1170A–1175A (1981).
19. M. Martin and P. S. Williams, in *Theoretical Advancement in Chromatography and Related Separation Techniques* (F. Dondi and G. Guiochon, Eds.), (NATO ASI Series C: Mathematical and Physical Sciences, Vol. 383), Kluwer Academic Publishers, Dordrecht, The Netherlands, 1992, pp. 513–580.
20. J. C. Giddings and M. N. Myers, *Sep. Sci. Technol.*, *13*, 637–645 (1978).
21. T. Koch and J. C. Giddings, *Anal. Chem.*, *58*, 994–997 (1986).
22. J. C. Giddings, X. Chen, K.-G. Wahlund, and M. N. Myers, *Ibid.*, *59*, 1957–1963 (1987).
23. S. K. Ratanathanawongs and J. C. Giddings, *J. Chromatogr.*, *467*, 341–356 (1989).
24. P. S. Williams, T. Koch, and J. C. Giddings, *Chem. Eng. Commun.*, *111*, 121–147 (1992).
25. P. S. Williams, S. H. Lee, and J. C. Giddings, *Ibid.*, In Press.
26. M. H. Moon, Ph.D. Thesis, University of Utah, 1992.
27. A. D. Maude, *Br. J. Appl. Phys.*, *12*, 293–295 (1961).
28. H. Brenner, *Chem. Eng. Sci.*, *16*, 242–251 (1961).
29. G. D. M. MacKay, M. Suzuki, and S. G. Mason, *J. Colloid Sci.*, *18*, 103–104 (1963).
30. R. G. Cox and H. Brenner, *Chem. Eng. Sci.*, *22*, 1753–1777 (1967).
31. M. D. A. Cooley and M. E. O'Neill, *Mathematika*, *16*, 37–49 (1969).
32. F. Durst and H. Raszillier, *Chem. Eng. Sci.*, *44*, 2871–2879 (1989).
33. P. Ganatos, S. Weinbaum, and R. Pfeffer, *J. Fluid Mech.*, *99*, 739–753 (1980).
34. A. J. Goldman, R. G. Cox, and H. Brenner, *Chem. Eng. Sci.*, *22*, 637–651 (1967).
35. M. E. O'Neill and K. Stewartson, *J. Fluid Mech.*, *27*, 705–724 (1967).

36. M. D. A. Cooley and M. E. O'Neill, *J. Inst. Math. Its Appl.*, *4*, 163–173 (1968).
37. P. Ganatos, R. Pfeffer, and S. Weinbaum, *J. Fluid Mech.*, *99*, 755–783 (1980).
38. P. Ganatos, S. Weinbaum, and R. Pfeffer, *Ibid.*, *124*, 27–43 (1982).
39. R. Hsu and P. Ganatos, *Ibid.*, *207*, 29–72 (1989).
40. R. Hsu and P. Ganatos, *Ibid.*, *268*, 267–292 (1994).
41. A. J. Goldman, R. G. Cox, and H. Brenner, *Chem. Eng. Sci.*, *22*, 653–660 (1967).
42. P. B. Canham and A. C. Burton, *Circ. Res.*, *22*, 405–422 (1968).
43. D. Danon and Y. Marikovsky, *J. Lab. Clin. Med.*, *64*, 668–674 (1964).
44. C. B. Fuh, S. Levin, and J. C. Giddings, *Anal. Biochem.*, *208*, 80–87 (1993).

Received by editor December 1, 1993